Characterization of hardness, elastic modulus and fracture toughness of RB-SiC ceramics at elevated temperature by Vickers test

Xiaoshuang Rao[1,2,3*], Feihu Zhang[1,2**], Xichun Luo[3], Fei Ding[3]

1 State Key Laboratory of Robotics and System (HIT), Harbin Institute of Technology, Harbin 150001, China

2 School of Mechatronics Engineering, Harbin Institute of Technology, Harbin 150001, China

3 Centre for Precision Manufacturing, DMEM, University of Strathclyde, Glasgow G1 1XQ, UK

[*]Corresponding author E-mail address: [*] rxs_cug@126.com; [**]fhzhang@hit.edu.cn

Abstract: In this paper, mechanical properties of RB-SiC ceramics, such as hardness, elastic modulus and fracture toughness, are characterized through indentation technique using a Vickers indenter at elevated temperatures ranging from room temperature to 1200 °C realized by laser heating. . The indentation size effect, load-displacement curves and relationship between crack length and applied load are studied in order to determine hardness, elastic modulus and fracture toughness accurately. The results show that the Meyer's index and Vickers hardness decrease with the increase temperature. It indicates that the permanent plastic deformation of RB-SiC ceramics is mainly responsible for the indentation size effect and the reduction of hardness at elevated temperature. Both material softening and plastic deformation will contribute to the indentation creep at elevated temperature as shown in the load-displacement curves. The elastic modulus decreases with the increase of temperature due to increase of contact depth as a result of less elastic recovery. In the indentation test for calculating fracture toughness, only radial-median cracks are identified by the relationship between crack length and applied load at all temperatures, although the fracture mode observed at the indent corner changes from transgranular at room temperature to intergranular at elevated temperature. As more energy is consumed by intergranular facture and cracking-

healing takes place due to oxidation, only short crack length appears in the indentation test which implies an increase of fracture toughness with the increase of temperature. However, this tendency has an exception at the highest temperature of 1200℃. This is because the free Si softening in RB-SiC specimen fails to resist crack propagation at extremely high temperature. Consequently, the crack length increases again which leads to the increase of the calculating fracture toughness at the highest temperature. These variations of hardness, elastic modulus and fracture toughness with temperatures will account for the possible change of material removal regimes occurred in some thermal-involved hybrid machining of RB-SiC ceramics.

Keywords: Vickers hardness; Elevated temperature; Elastic modulus; Fracture toughness; RB-SiC ceramics

1. Introduction

Reaction-bonded silicon carbide (RB-SiC), as one of the most prosperous material for substrate of lightweight space optical mirrors [1,2], is very difficult to machine because of its high hardness and brittleness. In recent years, some thermal-involved hybrid processes, such as laser assisted machining [3-5], ultrasonic assisted electrical discharge machining [6,7], ED milling and mechanical grinding compound process [8-10] and electrical discharge diamond grinding [11], have been attempted to improve the machinability of SiC ceramics. However, the thermal effect in these processes has a significant influence on the mechanical property of the machined surface material, which will change the material removal mode in the hybrid machining process, especially in the hybrid process combined with a mechanical action such as milling, turning and grinding. Therefore, variation of mechanical properties such as hardness, elastic modulus and fracture toughness at elevated temperatures should be firstly investigated for RB-SiC ceramics as they have direct influence on material removal mode.

Indentation technique has been considered as an effective method to obtain mechanical properties of sintered ceramics [12-14]. It primarily consists of performing an impression on the specimen surface by the penetration of a hard indenter at a given load. The mechanical properties are then determined by analysing the geometrical dimensions of the residual impression, the load-displacement curves during the indentation and the relative crack length at the indent corner. Pyramidal indenters such as Vickers indenter and Knoop indenter are generally used in the indentation test to measure hardness, elastic modulus and fracture toughness. Whereas ceramic generally has a lower Knoop than Vickers hardness due to the elastic recovery occurring around the Knoop indentation [15]. The extra work is consequently necessary to obtain the same hardness number with Vickers since Knoop hardness is actually the average contact pressure over the projected contact area rather than the true contact area [16,17]. Therefor, the Vickers indentation may be the best choice for hardness indentation. However, the elastic modulus and fracture toughness in Vickers indentation were reported to depend on the applied load and the number of radial cracks generated around Vickers impression, respectively [18,19]. The Vickers hardness was also found to increase with the decrease of test load and/or depth [13,20,21]. This phenomenon, named as indentation size effect (ISE), has been widely reported in existence in indentation test for ceramics [22-24] although the hardness, elastic modulus and fracture toughness, as the intrinsic properties of materials, are supposed to be independent of the applied load [15,19,25]. In order to obtain unique values of the mechanical properties, the proportional specimen resistance (PSR) and the modified PSR model were developed to determine the load-independent values of the mechanical properties [23,26].

However, research on mechanical properties of RB-SiC ceramics, up to date, mainly focus on the influence of microstructure [27,28], annealing treatment [29,30] and carbon perform [31] during the material fabrication. These investigations were generally conducted at room

temperature with a conventional measuring technique. Even though there were a few studies on the temperature-dependent mechanical behaviours for RB-SiC ceramics, they mainly focused on the strength and toughness with respect to the feasibility in application of temperature-required environment [32,33]. The hardness, elastic modulus and fracture toughness of RB-SiC ceramics at elevated temperatures have not been fully investigated. Nevertheless, the mechanical properties of RB-SiC ceramics will be influenced considerably by material softening and deformation induced by high temperature. RB-SiC ceramic is known to consist of SiC phase and free Si phase. The residual Si phase plays a great role on the onset of ductile behaviour, particularly at high temperature, because of the fact that Si is more plastic than SiC [34]. Consequently, a change in mechanical properties of RB-SiC ceramics might be induced by high temperatures.

Therefore, this paper carries out Vickers indentation test in order to gain understanding of the influence of elevated temperatures on hardness, elastic modulus and fracture toughness of RB-SiC ceramics. Considering the indentation size effect in the indentation test, the proportional specimen resistance model, load-displacement curve and relationship between crack length and applied load will be obtained to determine the values of load-independent hardness, elastic modulus and fracture toughness of RB-SiC ceramics at elevated temperatures. The indentation size effect, indentation creep and fracture mode will also be revealed to obtain underlying mechanism of the variation of hardness, elastic modulus and fracture toughness with temperatures.

2. Material and method

2.1 Sample preparation

Commercial RB-SiC ceramic supplied by Goodfellow Cambridge Ltd. (UK) was cut into small blocks with dimensions of 10mm×10mm×6mm by wire electrical discharge machining.

Each block was then polished with diamond slurries of 5μm,0.5μm and 0.25μm step by step until a smooth and below 50nm (SRa) surface-finish was accomplished. The polished specimens were firstly cleaned with deionized water and then ultrasonic cleaned with 95 vol.% medical alcohol for the following indentation tests and detections. Microstructurally the RB-SiC material contained SiC, residual Si and a minor amount of porosity, shown as the micromorphology of the polished surface in Fig.1. The ratio of porosity was estimated to be 2.5% based on the calculation of the area of the porosity. The content of the residual Si, provided in the Goodfellow official website [35], is 10 vol.%. Other material properties of the RB-SiC ceramics such as Vickers hardness, tensile modulus and upper continuous use temperature that may relate to the investigation as references are 25-35GPa, 410GPa and 1350℃, respectively.

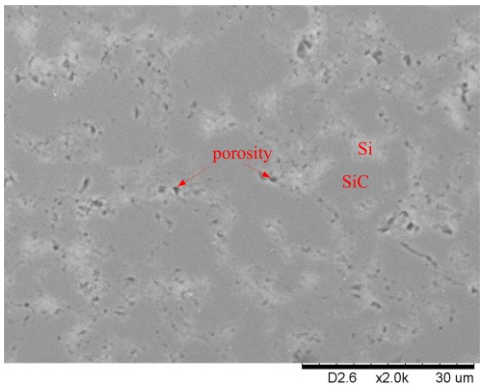

Fig.1 Micromorphology of the polished surface of RB-SiC ceramic

2.2 Vickers indentation test

The Vickers indentation tests were performed on an ultra-precision machine-micro-3D with a fibre-laser for heating the SiC specimen, as shown in Fig.2 (a). The Vickers indenter HV-3 (Shanghai Liheng, Co., Ltd, China) at loads of 0~50*kgf* was employed to produce indents. A current-controlled linear guide rail was used to apply the load through NC program, which enables the minimum displacement of 0.1μm and maximum load up to 40N. The measurement cell in the machine was used to record the position of the indenter, which can

detect displacement change as small as 1nm. The Vickers indenter, with include angles of 136° between opposite faces and 148° between opposite edges, was fixed on the linear guide rail by rigid connection. The load was measured by a three-component piezoelectric dynamometer (Kistler 9129 AA) with resolution of 1mN.

Priors to trails, relationships between the laser power and the resultant temperature on the surface of RB-SiC specimen was firstly measured with an infrared thermometer (IR-750-EUR, USA). The temperatures varying with heated time at different laser powers were collected by the IR-750 software in PC, plotted in Fig.2(b). Consideration of graphitization temperature (900℃) of diamond and upper continuous use temperature (1350℃ [35]) of the commercial RB-SiC ceramic, four different laser powers of 20W, 40W, 80W and 160W were selected to heat the RB-SiC specimens to corresponding temperatures of 200℃, 600℃, 900℃ and 1200℃, respectively. In order to minimize the thermal drift caused by contact between cold indenter and heated specimen, the specimen-indenter was kept in contact during the heating process before the indentation.

Considering the possible ISE in the tests, eleven different maximum loads ranging from 0.25N to 19.62N, with increasements of 0.05*kgf* from 0.25N up to 0.98N, 0.1*kgf* from 0.98N up to 4.91N and 0.5*kgf* from 4.91N up to 19.62N respectively, were selected for the indentation tests. All tests were performed with a 10s holding time and 30s loading-unloading period. At each load, five indents were made to determine the hardness and fracture toughness. Moreover, a maximum load of 1N was used to test the elastic modulus at different temperatures. By comparison, a contrast indentation test was also conducted at room temperature (RT, 23.7℃).

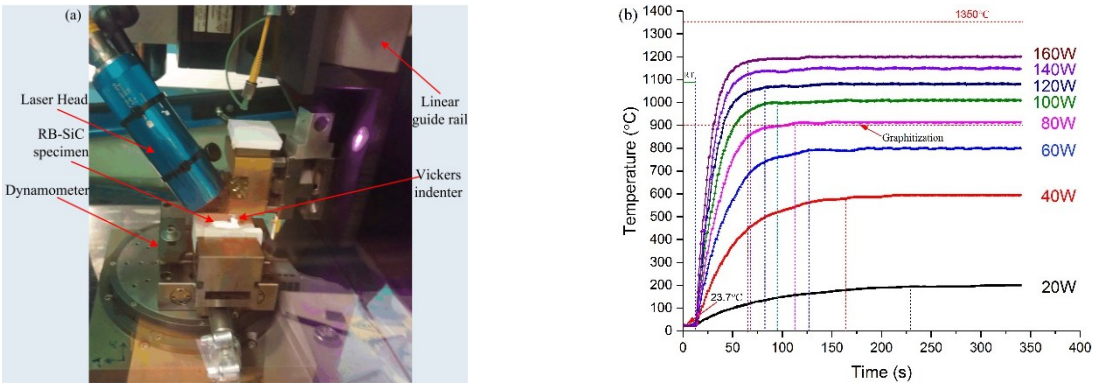

Fig.2 Details of the experiments. (a) Setup of the experiment (b) Relationship between laser power and the resultant temperature on surface of RB-SiC specimen.

2.3 Sample characterization and measurement

The residual indentation impressions at different loads and temperatures were imaged by scanning electron microscope (SEM) (TM-1000, Hitachi, Japan). The two diagonals of the square shaped impression were then measured by image analysis software (Digimizer, Belgium). The cracks mainly generated at the corners of the residual indentation impressions were also measured in the same way. The averages of diagonal and crack length at particular load were calculated for 5 indents. The variations of applied load and displacement were also recorded by a measurement cell assembled on the machine to determine the elastic modulus of RB-SiC ceramic at different elevated temperatures.

3. Results and discussion

3.1 Analysis of residual indentation impression

The residual indentation impressions at different temperatures and the load of 19.62N were shown in Fig.3. Fractures occurred at the edge of the residual indentation impression. At room temperature, the fracture morphology with appearance of smooth and planar cleavage facets was suggested as transgranular failure in Huang et al.'s work [33]. Moreover, massive microcracks are roughly parallel to the edges of the residual impression, which indicates that

the brittle fracture mode dominates in room temperature indentation. However, fracture occurred at elevated temperature trends to more cleavage facets with relative smaller area as well as some holes due to the pullout of SiC particles. Material pile-up is visible on the edges of the residual indentation impression coupled with particles or fragments. More importantly, the material pile-up trends to increase with the increase of temperature. Covering with small oxide particles, the surface of residual indentation impression appears more ductile deformation at elevated temperature rather than microcracks parallel to the edges at room temperature. Besides, the average diagonal length of the indentation impression roughly increases with the increase of temperature. Thus, it can be concluded that the high temperature softens the RB-SiC material and will result in a decrease of hardness, which may be helpful for machining of the RB-SiC ceramics in ductile regime.

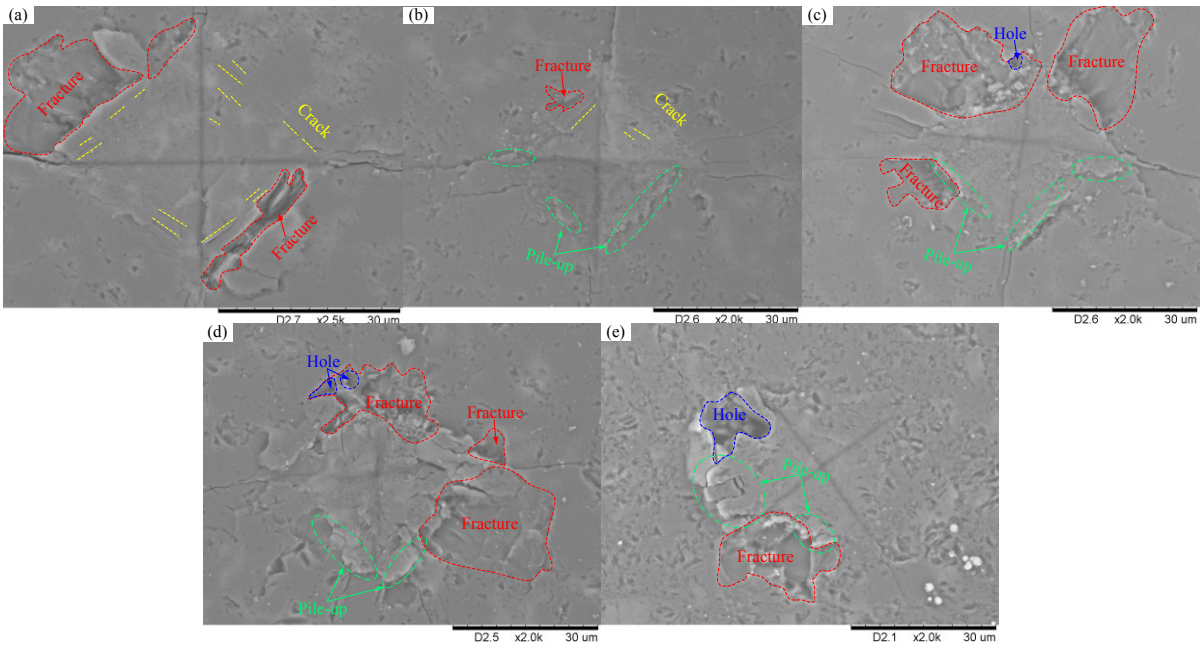

Fig.3 Morphology of residual indentation impressions at different temperatures and the load of 19.62N. (a) RT, (b)200℃, (c) 600℃, (d)900℃and (e) 1200℃

3.2 Vickers hardness and the indentation size effect affected by temperature

The hardness of a material represents its resistance to plastic deformation usually by indentation [12]. The general relation to calculate the Vickers hardness is determined by the ratio of the applied load via a geometrical indenter of defined shape to the contact projected area [13,36]:

$$H_v = 1.8544 \times 10^3 \, P/d \tag{1}$$

Where H_v is the Vickers hardness in GPa, P is the applied load in Newtons and d is the average value of the two diagonal lengths for each Vickers indentation impression in μm. Thus, the Vickers hardness values were calculated and plotted in Fig. 4 based on the measurements of the diagonal at a relatively wide range of applied loads.

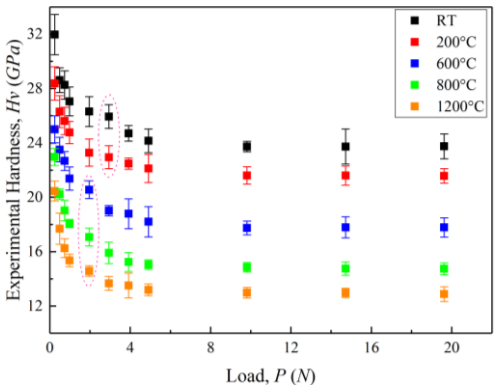

Fig.4 Vickers hardness varied with applied load

Here, each of plotted data points and its error bar are the averages of five indent measurements and their standard deviations, respectively. It is clearly evident that, at all temperatures, the experimental Vickers hardness decreases dramatically with an increase of loads at the lower range of loads. It then trends to stable values at the higher range of loads, which implies that the ISE occurs in all temperature indentation tests. The classical Meyer's law is usually utilized to evaluate the ISE by analysing the relationship between the Meyer's index n and 2, which is given by [13,23]:

$$P = Ad^n \tag{2}$$

The constant A and Meyer's index n can be derived directly from the regression fitting of $\ln P$ (in Newton) versus $\ln d$ (in μm), plotted in Fig.5. The Meyer's index n is the slope of the regression line, and the ISE is usually related to the deviation of the n-value form 2 [23]. Note that the higher deviation is below 2, the more significant ISE will be obtained. And the ISE is absence when n is equal to 2. The Meyer's indexes in present work are summarized in Table 1. According to the different decreasing rates of the hardness via the increasing applied load, each experimental data in present work displays linear relationship with two n-values for two different ranges of loads. The similar results were also reported in Roy's work [13].

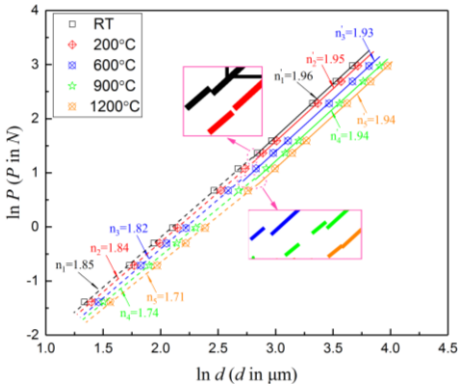

Fig. 5. $\ln P$ versus $\ln d$ fitting curves at different temperatures

Table 1 Meyer's index obtained by fitting the load-hardness variation at different ambient temperatures

Ambient temperature	Slop		
	n_i	n_i'	n
RT	1.85	1.96	1.88±0.01
200°C	1.84	1.95	1.88±0.01
600°C	1.82	1.93	1.84±0.01
900°C	1.74	1.94	1.82±0.02
1200°C	1.71	1.94	1.82±0.02

It should be noted that, at the low range of load for a particular temperature test, all the *n*-values are lower than those at high loads, which implies that more significant ISE occurs easily at low loads. While the *n*-value at higher load are close to 2 in all temperature tests, which indicates minimal presence of ISE in the hardness data. Due to ISE is considered to be generated as a result of the proportional elastic resistance of the specimen under the load [13], elastic recovery trends to develop more significantly at low range of loads because of the nature of intrinsic brittleness of RB-SiC ceramics. Moreover, the low range of loads (~1.96N marked with dotted line frame in Fig.4) show a slight decrease at higher temperature compared with those (~2.94N) at room temperature and 200℃. This is attributed to more plastic deformation at elevated temperatures, which will reduce the ISE to a lower load. However, the Meyer's index n, including the values of both the two ranges of applied loads and the whole range of loads at a particular temperature, shows a slight decline with the increase of the temperatures. It signifies the increase of the ISE with the increase of temperatures. The dislocation-based obstacles may be responsible for the temperature dependence of the ISE, since the indentation would involve dislocation multiplication and lead to a higher density of statistically stored dislocations at elevated temperatures [37]. Consequently, the decrease in the plasticity length scale induced by accumulation of dislocation results in the increase of the ISE. Therefore, a load-independent hardness, sometimes referred to "true hardness" [23], is necessary to assess the material properties of RB-SiC reasonably and accurately.

A proportional specimen resistance (PSR) model proposed by Li and Bradt [26] and a modified PSR model proposed by Gong et al. [23] are a widely used approach in calculation of the true hardness. The former takes the elastic resistance of the specimen and frictional effects between the indenter and specimen into consideration. While the latter adds additional consideration on permanent deformation of the test specimen during indentation. However,

the applied load P and the resultant indentation dimension d are both predicted to follow the relationships in these two models

$$P = a_1 d + a_2 d^2 \tag{3}$$

$$P = P_0 + a_1 d + a_2 d^2 \tag{4}$$

The coefficient a_1 and a_2 in PSR model (equation (3)) are determined by fitting of P/d versus d. And it is generally acknowledged that a_2 term directly denotes the load-independent hardness while a_1 term is believed to relate to the degree of cracking induced by indentation underneath and around the residual impression [18]. In modified PSR model (equation (4)), the coefficient a_1 and a_2 keep the same physical meanings as the PSR model, but they are evaluated through fitting by a polynomial regression. The P_0 was suggested to relate to the residual surface stress in the test specimen [18]. The plots of PSR model and modified PSR model are shown in Fig.6.

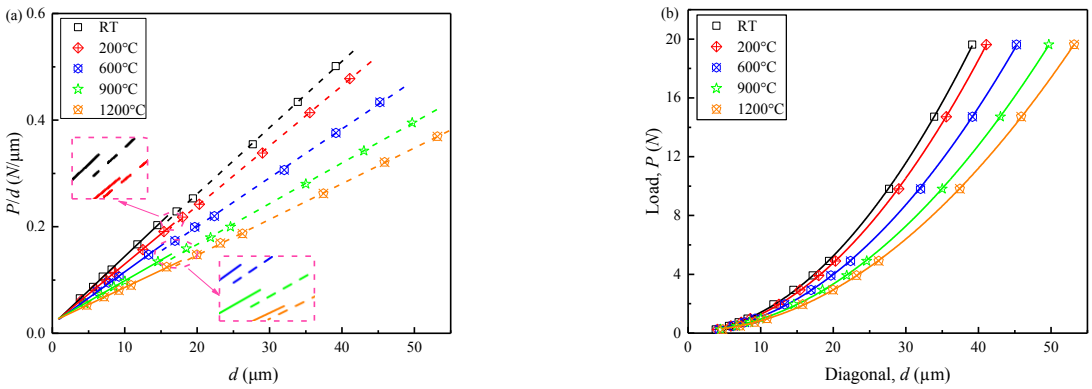

Fig.6 Fitting curves for RB-SiC ceramics at different temperatures. (a) PSR model by fitting of P/d versus d (b) modified PSR model fitted by polynomial regression

For the PSR model, all data at a particular temperature fall into two separated parts as shown in Fig.6 (a), and both of them show apparent linearity. They are similar to the curves fitted with the Meyer's law shown in Fig.5. Two different a_2 values signify two different true hardness at the particular temperature for the RB-SiC material. But it is unreasonable for a

given material characterized with two or more different true hardness [23]. Thus, the PSR model is unsuitable to provide a satisfactory explanation of load-independent hardness in present work as it cannot describe the ISE absolutely in the elevated temperature indentation. Therefore, the modified PSR model was applied in calculation of the load-independent hardness. Fig.6 (b) shows well-fitting of the experimental data with the modified PSR model, and their coefficients are summarized in Table 2. The load-independent hardness, namely the true hardness, were also calculated according to the coefficient a_2 at different elevated temperatures. It is clearly evident that the load-independent hardness decreases with increase of the temperature, and the hardness even decreases by 46.1% at 1200℃ compared with that at room temperature. The decrease of the true hardness can be attributed to the plastic deformation at elevated temperature because the modified PSR model takes material permanent deformation into consideration, which agrees well with the phenomenon of material pile-up and decreasing cracks detected in residual indent micromorphology of RB-SiC sample. As for covalent crystals, the motion of dislocation with directed interatomic bonds is obstructed by bending and turning of the bonds in the crystal lattice, the stress required for the motion of dislocation with thermal oscillation will be lower [38]. The facilitated dislocation results in the material pile-up and the decrease of hardness.

Table 2 Results of the P_0, a_1 and a_2 terms fitted by modified PSR model and load-independent hardness.

Temperature (℃)	P_0 (N)	a_1 (N/mm)	a_2 (N/mm^2)	True hardness (GPa)
RT	0.0709	9.2	12500	23.18±1.85
200℃	0.0601	8.8	11400	21.14±0.56
600℃	0.1090	7.3	9300	17.25±1.11
900℃	0.1233	5.6	7800	14.46±0.75
1200℃	0.0978	6.8	6800	12.61±0.74

3.3 Elastic modulus at elevated temperature

Elastic modulus is another important property related to the material removal in machining of hard and brittle materials. It can be estimated from the load-displacement curve using Oliver and Pharr methods [39]. A reduce modulus E_r was defined to take into account for the effects of non-rigid indenters on the load-displacement behaviour which can be described as:

$$\frac{1}{E_r} = \frac{1-\nu_s^2}{E_s} + \frac{1-\nu_i^2}{E_i} \tag{5}$$

Where E_s and ν_s are elastic modulus and Poisson's ratio of the specimen. E_i and ν_i are elastic modulus and Poisson's ratio of indenter, which are 1141GPa and 0.07 for diamond indenter, respectively. Besides, the reduced modulus can also be determined by analysing the load-displacement curve according to the following equation:

$$E_r = \frac{S}{2} \cdot \sqrt{\frac{\pi}{A_c}} \tag{6}$$

Where A_c is the projected area of contact at maximum load, S is the experimental measured stiffness of the upper portion of the elastic unloading. S can be determined through calculating the slop of the load-displacement curve at the beginning of unloading process, namely $S = dP/dh$ as shown in Fig.7.

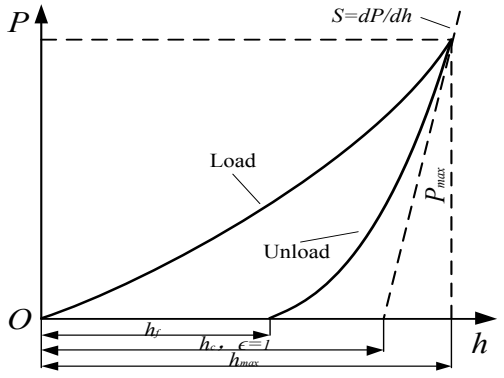

Fig.7 A schematic representation of load versus indenter displacement

For Vickers indenter, the projected area can be calculated by the contact depth according to the given geometry:

$$A_c = 4h_c^2 \tan\left(\frac{\alpha}{2}\right) = 24.5h_c^2 \tag{7}$$

In the relationship of load and displacement for indenter, the contact depth h_c is determined by

$$h_c = h_{max} - \varepsilon \frac{P_{max}}{dP/dh} \tag{8}$$

Where h_{max} is the maximum depth determined experimentally, ε is a constant that depends only on indenter geometry, and $\varepsilon = 0.75$ for a Vickers indenter [39-41].

In this paper, a maximum load *1N* was applied to determine the elastic modulus at elevated temperature. The load-displacement curves and the variations of indentation depths at different temperatures are shown in Fig.8. Different from curve at room temperature shown as Fig.8 (a), load-displacement curves at elevated temperatures creep during the holding duration of the maximum load. It is clearly that the load keeps constant while the depth of indenter increases during the holding duration. This is mainly attributed to plastic deformation of the RB-SiC specimen at elevated temperature. The occurrence of indentation creep under constant load was also reported in Kim and Heuer's work [40], where less elastic recovery was suggested at high temperature than that occurred at room temperature. In addition, the plastic behaviour of indentation presents an increasing tendency with increase of the temperatures, seeing the increment of the contact depth Δh_c (the deviation from the contact depth at room temperature) at elevated temperature and indentation creep depth h_T shown in Fig.8(b). The identical trends of Δh_c and h_T imply softening and plastic deformation with the increase of temperatures, which may cause the decrease of the elastic modulus at elevated temperatures.

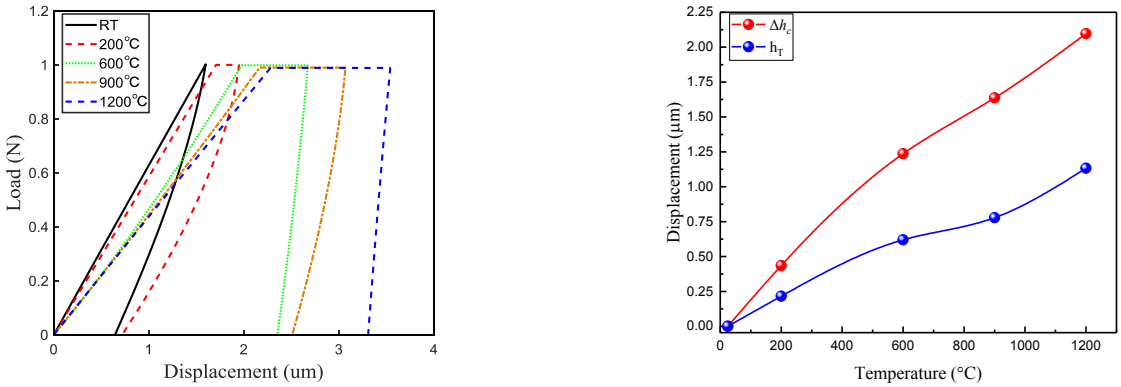

Fig.8 Load-displacement curves and the variations of indentation depths at different temperatures. (a) the load-displacement curves and (b) the variations of indentation depths

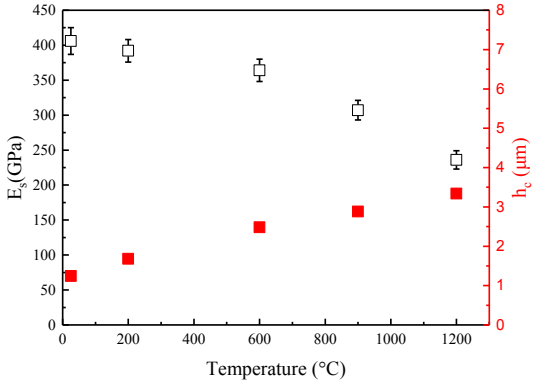

Fig.9 Elastic modulus and contact depths at different temperatures

Fig.9 presents the elastic modulus and contact depths at different temperatures. With increase of temperatures, the contact depth h_c calculated by equation (8) increases due to indentation creep results in a larger h_{max}. Consequently, the elastic modulus decreases with the increase of temperatures. Compared with the average elastic modulus of 406.6GPa±19.0GPa for the RB-SiC specimen at room temperature, the average elastic modulus of 236.6GPa±13.1GPa at 1200℃ has decrease by 41.8%. The deteriorated elastic modulus at elevated temperature is almost the same magnitude to the deteriorated load-independent hardness, which is in accord with the results reported by Liu et al [42]. The material thermal softening and amorphization are responsible for deteriorated hardness and elastic modulus owing to the unrecovered deformation or displacement at elevated temperature.

3.4 Fracture toughness

In Vickers indentation method, the fracture toughness measurement is mainly based on the cracks generated at the corner of the indentation impression. Fig.10 shows the typical crack systems in Vickers indentation fracture (VIF) test. The cracks remained connection to the corner of the indentation marks were suggested as the redial-median cracks while the cracks detached from the corner of indentation were treated as the Palmqvist cracks [25,36,43]. And there are different equations to calculate the fracture toughness for different crack systems in VIF test, which are given by [12,25]:

For radial-median crack:
$$K_C = 0.0154\left(\frac{E}{H_v}\right)^{1/2}\left(\frac{P}{c^{3/2}}\right) \tag{9}$$

For Palmqvist crack:
$$K_C = 0.0089\left(\frac{E}{H_v}\right)^{2/5}\left(\frac{P}{a\cdot l^{1/2}}\right) \tag{10}$$

Where a is the diagonal half length, c and l are the crack lengths initiated at the centre and the tip of indentation impression, respectively. Thus, the types of cracks at the indent corner should firstly be determined.

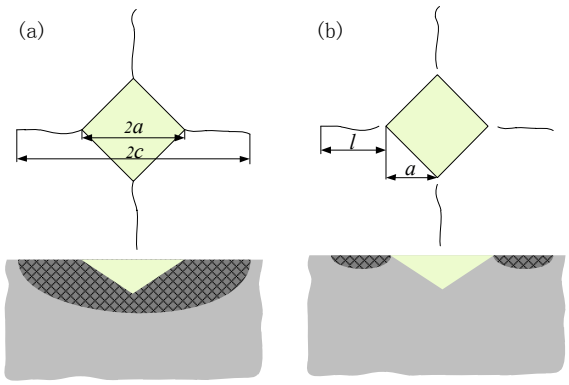

Fig.10 Typical crack systems in Vickers indentation fracture test. (a) Radial-median crack and (b) Palmqvist crack

In present work, the cracks generated around the residual indentation impression at different temperatures and same load are presented in Fig.11. A crack system, including cracks initiated at the corner of the indent and the cracks apparently separated from the corner of the indent, is observed on all surfaces of the RB-SiC specimens at different ambient temperatures. Differing from that a continue crack propagation is detected on the surface of RB-SiC specimen in room temperature VIF test, the cracks initiated at the indent corner seem to have an interrupting propagation in elevated temperature VIF test, shown in the magnified morphology at the upper-right corner of Fig.11. The distance, from where the crack propagation was interrupted to the indent corner, decreases with the increase of temperatures. This may be attributed to a change in fracture mode of RB-SiC material at elevated temperatures, which is from a dominant transgranular fracture at room temperature to a dominant intergranular fracture at elevated temperature. Due to the excessive softening of amorphous film, the Si/SiC interface bonding energy trends to decrease with increase of temperatures, resulting in a deterioration of interface bonding strength between Si and SiC grains [34], which easies the intergranular fracture. As a result, the location of the fracture mode changed from transgranular to intergranular movies towards the indent corner with the increase of temperatures. However, the types of cracks at the indent corner can still not be determined accurately just by the observations because it need to polish the surface layer away to make sure where the crack is actually generated [43].

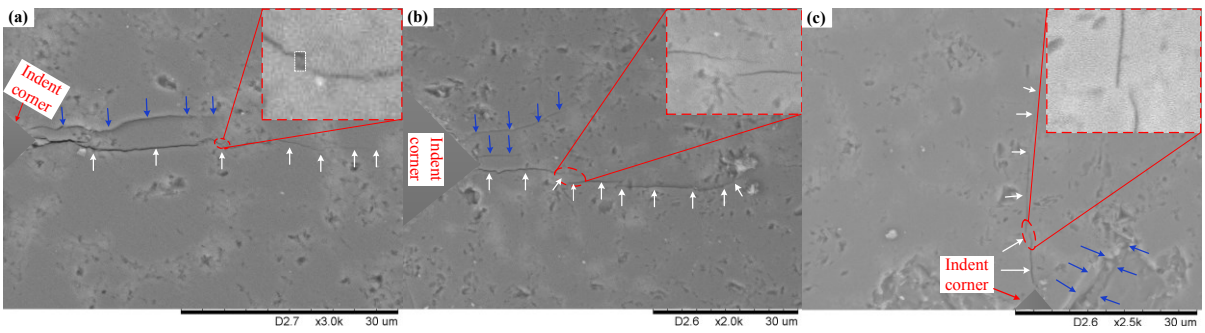

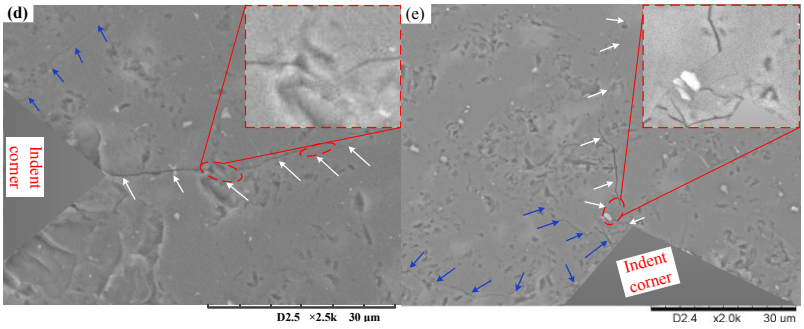

Fig.11 Cracks at the indent corner at different temperature. (a) RT, (b)200℃, (c)600℃, (d) 900℃ and (e) 1200℃

In order to obtain a unique fracture toughness value, the VIF test of RB-SiC specimens should be conducted at a suitable applied load to satisfy the ratio of crack length c to diagonal half-length a, that is, it is usually $c/a \gg 2$ [44]. The relationship between the crack length and diagonal half-length at the range of the applied loads from 1.96N to 19.62N are plotted in Fig.12 (a). Except for 1200℃, the crack length decreases with the increase of temperatures although the diagonals keep increase because of material softening and plastic deformation at all applied loads. That the melting and vaporization of the free Si phase because of local temperature over the melting point of the free Si leading to defects in RB-SiC specimen may be responsible for the crack length increase again at average temperature of 1200℃. Nevertheless, the ratio of crack length to diagonal half-length at all applied load is a constant for a particular temperature. It indicates that a unique fracture toughness can be obtained at different temperatures. However, Chicot et al. [25] suggested that a suitable application of equations (9) and (10) should require another condition on the different load to crack length criterion ratios. In addition, they held the view that the parameters $P/c^{3/2}$ and $P/al^{1/2}$ should be obviously constant in order to obtain a unique toughness value. Taking the ISE into consideration, the two crack lengths, c and l, were represented as a function of the applied load in bi-logarithmic coordinates to determine the types of crack systems at different temperatures. The theoretical slop of $\ln P$ versus $\ln c$ is 2/3 for radial-medial crack while the

theoretical slop of $\ln P$ versus $\ln l$ is 2(1-1/n) for Palmqvist crack. Fig.12 (b) shows the fitting curves of $\ln P$ versus $\ln c / \ln l$ in room temperature VIF test. By comparison, the crack system can be determined as the radial-median crack. Similarly, the slops of $\ln P$ versus $\ln c / \ln l$ at elevated temperature were summarized in Table 3. It is clear that all cracks at different temperatures are the radial-median cracks. Thus, the equation (9) should be selected to calculate the facture toughness of RB-SiC specimens in all temperature indentation tests.

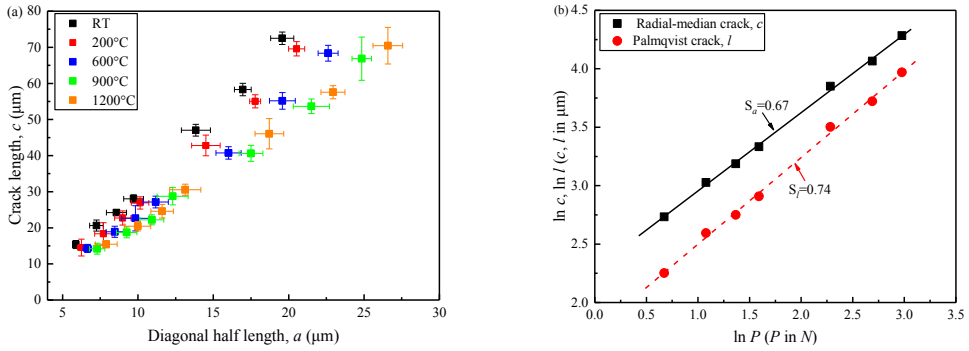

Fig.12 Relationships between the applied load P and the diagonal half-length a or the crack length c. (a) relationship between a and c (b) relationship between $\ln P$ and $\ln c / \ln l$ and their fitting curves in room temperature VIF test.

Table 3 Theoretical and experimental slopes of the crack length c or l versus the applied load P in bi-logarithmic coordinates to determine the types of cracks

Crack type	S_i	RT	200℃	600℃	900℃	1200℃
Radial-median	$c \propto P^{2/3}$	2/3	2/3	2/3	2/3	2/3
	$c = f(P)$	0.67 ± 0.01	0.68 ± 0.01	0.67 ± 0.01	0.66 ± 0.02	0.65 ± 0.02
Palmqvist	$l \propto P^{2(1-1/n)}$	0.94	0.94	0.91	0.90	0.90
	$l = f(P)$	0.74 ± 0.02	0.77 ± 0.01	0.76 ± 0.02	0.75 ± 0.04	0.76 ± 0.03

According to the analysis above, the fracture toughness values variated with the applied load were calculated by equation (9) and plotted in Fig.13 (a) at all temperatures. Considering the possible effect of applied load on fracture toughness induced by elevated temperature, a range of loads from 1.96N to 19.62N was taken to test the fracture toughness at each temperature. Obviously, the fracture toughness basically holds a stable value for a given temperature. In other word, the fracture toughness does not vary with the applied load, which indicates the validity of the results for the fracture toughness as it is exclusive for a given material at a particular temperature. The averages of fracture toughness under different applied loads are treated as the final fracture toughness at a particular temperature, plotted with its error bar in Fig.13 (b). The fracture toughness presents an increasing trend with the increase of temperatures except for 1200℃. This is attributed to the material softening below 1200℃, resulting in shorter crack generated because of the increase of plastic deformation. The variation trend of fracture toughness with temperature matches well with the reported results [33] although the maximum temperature for fracture toughness turning to decline because of the different free Si-content and the average of the temperature actually obtained in the tests. Moreover, the variation trend of fracture toughness with temperature also agrees with the variation of the coefficient a_1 obtained in Section 3.2, which indicates proportional greater contact damage through cracking with larger a_1 [18].

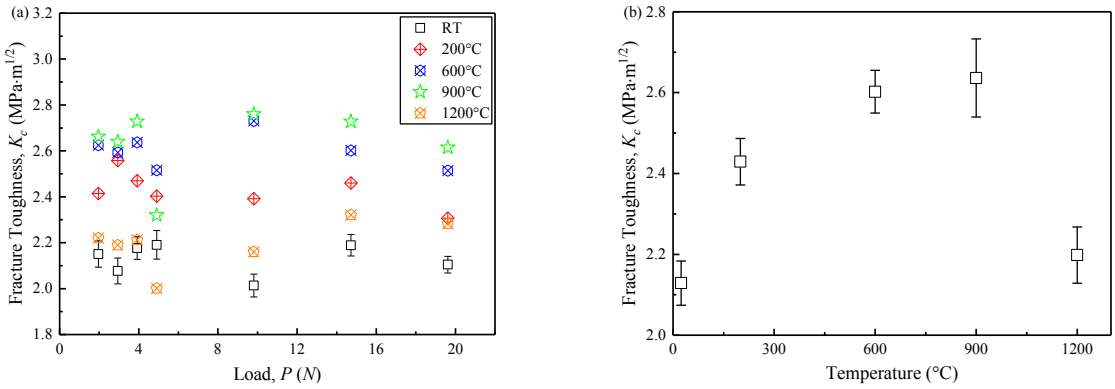

Fig.13 Variations of fracture toughness with different loads at different temperatures and their averages varied with temperatures. (a) fracture toughness at different temperatures (b) averages of the fracture toughness with error bars varied with temperatures.

For intergranular fracture, larger fracture energy than transgranular fracture is consumed [28]. This intergranular fracture contributes to toughening in brittle material [33, 45]. Meanwhile, the cracks in RB-SiC ceramics can be healed by filling amorphous silica produced by the oxidation of silicon and silicon carbide [46]. Thus, only short crack length will be generated at elevated temperature as majority of fracture energy has been consumed in the crack filling process and t it is not enough to generate a long crack during the propagation. As a result, an increasing fracture toughness value was obtained for RB-SiC ceramics at elevated temperature. However, extremely high temperature makes it difficult to resist crack propagation due to the softening of free Si [33], resulting in the decrease of fracture toughness at 1200℃.

4. Conclusions

In the present work, the indentation tests were conducted to explore the influence of elevated temperatures on the mechanical properties of RB-SiC ceramics, such as hardness, elastic modulus and fracture toughness. A comparative test was also conducted at room temperature. Based on the results and discussion, the main conclusion could be summarized as follows:

(1) The Vickers hardness decreases with the increase of applied load at a particular temperature, showing a remarkable load-dependence, namely the indentation size effect. Thus, the Meyer's index was used to assess the degree of the ISE at different load ranges and temperatures. The results show more significant ISE at low range of loads and high temperature. The elastic recovery is responsible for the ISE at lower range of loads while the dislocation-based obstacles are responsible for the ISE at high temperatures. It

indicates plastic deformation caused by dislocation is the main reason of the ISE at high temperatures.

(2) The true hardness fitted by the modified PSR decreases with the increase of temperatures. Because the PSR model failed to obtain the unique true hardness, the modified PSR model was then taken to calculate the load-independent hardness at different temperatures by taking the plastic deformation into consideration. The true hardness decreases by 46.1% at 1200℃ compared with that at room temperature. Besides, the variation of the first-coefficient of the modified PSR model with temperatures indicates a contact damage induced by cracks with initiated increasing and then decreasing tendency.

(3) In contrast to the load-displacement curve at room temperature, the load-displacement curves at elevated temperatures occur indentation creep at the maximum load because of the increase of plastic deformation. The contact depth between indenter and RB-SiC specimen and indentation creep both increase with the increase of temperatures, resulting in the decrease of the calculating elastic modulus using Oliver and Pharr methods. Moreover, the variation of elastic modulus with temperature is similar to Vickers hardness, which decreases by 41.8% with the same declining magnitude of the Vickers hardness at 1200℃.

(4) A crack system changed from transgranular at room temperature to intergranular at elevated temperature was firstly discovered at the corner of the indent. The crack system was then identified as the radial-median crack according to the relationship between the crack length and the applied load. Thus, the equation for radial-median crack was selected to calculate the fracture toughness. The calculating fracture toughness initially increases and then decreases with the increase of temperatures, which are attributed to different fracture energy consumption and free Si softening.

Acknowledgements

This work was supported by the National Key Research and Development Program of China (2016YFB1102204), the Self-Planned Task (SKLRS201717A) of State Key Laboratory of Robotics and System (HIT) and the National Key Basic Research and Development Program of China (973 program, Grant No.2011CB013202). The authors also gratefully acknowledge the financial support from the EPSRC (EP/K018345/1) for this study. We would like to express our gratitude to Dr. Yukui Cai who has offered us valuable suggestions during our studies.

References

[1] K. Tsuno, H. Irikado, K. Hamada, O. Kazuhiko, J. Ishida, S. Suyama, Y. Itoh, N. Ebizuka, H. Eto, Y. Dai. Reaction-sintered silicon carbide: newly developed material for lightweight mirrors, 5th Int Conf Space Opt. 554 (2004) 681–685.

[2] S. Suyama, T. Kameda, Y. Itoh. Development of high-strength reaction-sintered silicon carbide, Diamond and related materials. 12 (2003) 1201-1204.

[3] Y. Hibi, Y. Enomoto, K. Kikuchi K, N. Shikata. Excimer laser assisted chemical machining of SiC ceramic, Applied physics letters. 66 (1995) 817-818.

[4] A.R. Shayan, H.B. Poyraz, D. Ravindra, J.A. Patten . Pressure and temperature effects in micro-laser assisted machining (μ-LAM) of silicon carbide, Transactions NAMRI/SME. 37 (2009) 75-80.

[5] A.R. Shayan, H.B. Poyraz, D. Ravindra, M. Ghantasala, J.A. Patten. Force Analysis, Mechanical Energy and Laser Heating Evaluation of Scratch Tests on Silicon Carbide (4H-SiC) in Micro-Laser Assisted Machining (μ-LAM) Process, American Society of Mechanical Engineers. 1 (2009) 827-832.

[6] P.J. Liew, K. Shimada, M. Mizutani, J. Yan, T. Kuriyagawa. Fabrication of Microstructures on RB-SiC by Ultrasonic Cavitation Assisted Micro-Electrical Discharge Machining, Int. J. of Automation Technology. 7(2013): 621-629.

[7] P.J. Liew, J. Yan, T. Kuriyagawa. Fabrication of deep micro-holes in reaction-bonded SiC by ultrasonic cavitation assisted micro-EDM, International Journal of Machine Tools and Manufacture. 76 (2014) 13-20.

[8] R. Ji, Y. Liu, Y. Zhang, B. Cai,X. Li, C. Zheng. Effect of machining parameters on surface integrity of silicon carbide ceramic using end electric discharge milling and mechanical grinding hybrid machining, Journal of Mechanical Science and Technology. 27 (2013) 177-183.

[9] R. Ji, Y. Liu, Y. Zhang, B. Cai, R. Shen. Electric discharge milling and mechanical grinding compound machining of silicon carbide ceramic, Machining Science and technology. 14 (2010) 502-521.

[10] R. Ji, Y. Liu, Y. Zhang, B. Cai, H. Li, J. Ma. Optimizing machining parameters of silicon carbide ceramics with ED milling and mechanical grinding combined process, The International Journal of Advanced Manufacturing Technology. 51 (2010) 195-204.

[11] X. Rao, F. Zhang, C. Li, Y. Li. Experimental investigation on electrical discharge diamond grinding of RB-SiC ceramics, The International Journal of Advanced Manufacturing Technology. 94 (2018) 2751-2762.

[12] D. Chicot, A. Tricoteaux. Mechanical Properties of Ceramic by Indentation: Principle and Applications, Ceramic Materials. InTech, (2010) ISBN978-953-307-145-9

[13] T.K. Roy. Assessing hardness and fracture toughness in sintered zinc oxide ceramics through indentation technique, Materials Science and Engineering: A. 640 (2015) 267-274.

[14] Z.S. Ma, Y.C. Zhou, S.G. Long, X.L. Zhang, C. Lu. Characterization of stress-strain relationships of elastoplastic materials: An improved method with conical and pyramidal indenters, Mechanics of Materials. 54 (2012) 113-123.

[15] G.B. Ghorbal, A. Tricoteaux, A. Thuault, G. Louis, D. Chicot. Comparison of conventional Knoop and Vickers hardness of ceramic materials, Journal of the European Ceramic Society. 37 (2017) 2531-2535.

[16] J. Gong, J. Wang, Z. Guan. A comparison between Knoop and Vickers hardness of silicon nitride ceramics, Mater. Lett. 56 (2002) 941–944

[17] D. Chicot, D. Mercier, F. Roudet, K. Silva, M.H. Staia, J. Lesage. Comparison of instrumented Knoop and Vickers hardness measurements on various soft materials and hard ceramics, J. Eur. Ceram. Soc. 27 (2007) 1905–1911.

[18] O. Sahin, O. Uzun, M. Sopicka-Lizer, H. Gocmez, U. Kölemen. Dynamic hardness and elastic modulus calculation of porous SiAlON ceramics using depth-sensing indentation technique, Journal of the European Ceramic Society. 28(2008) 1235-1242.

[19] J. Wade, S. Ghosh, P. Claydon, H. Wu. Contact damage of silicon carbide ceramics with different grain structures measured by Hertzian and Vickers indentation, Journal of the European Ceramic Society. 35 (2015) 1725-1736.

[20] Y.V Milman, A.A. Golubenko, S.N. Dub. Indentation size effect in nanohardness, Acta. materialia. 59 (2011) 7480-7487.

[21] M.M. Renjo, L. Ćurković, S. Štefančić, D. Ćorić. Indentation size effect of Y-TZP dental ceramics, Dental Materials. 30 (2014) e371-e376.

[22] P. Maiti, M. Bhattacharya, P.S. Das, P.S. Devi, A.K. Mukhopadhyay. Indentation size effect and energy balance issues in nanomechanical behavior of ZTA ceramics, Ceramics International. 44 (2018) 9753-9772.

[23] J. Gong, J. Wu, Z. Guan. Examination of the indentation size effect in low-load Vickers hardness testing of ceramics, Journal of the European Ceramic Society. 19(1999) 2625-2631.

[24] Z. Peng, J. Gong, H. Miao. On the description of indentation size effect in hardness testing for ceramics: Analysis of the nanoindentation data, Journal of the European Ceramic Society. 24 (2004) 2193-2201.

[25] D. Chicot, G. Duarte, A. Tricoteaux, B. Jorgowski, A. Leriche, J. Lesage. Vickers Indentation Fracture (VIF) modeling to analyze multi-cracking toughness of titania, alumina and zirconia plasma sprayed coatings, Materials Science and Engineering: A. 527 (2009) 65-76.

[26] H. Li, R.C. Bradt. The microhardness indentation load/size effect in rutile and cassiterite single crystals, Journal of Materials Science. 28 (1993) 917-926.

[27] O.P. Chakrabarti, S. Ghosh, J. Mukerji. Influence of grain size, free silicon content and temperature on the strength and toughness of reaction-bonded silicon carbide, Ceramics International. 20 (1994) 283-286.

[28] B.K. Jang, S.Y. Kim, I.S. Han, D.W. Seo, K.S. Hong, S.K. Woo, Y. Sakka. Influence of uni and bi-modal SiC composition on mechanical properties and microstructure of reaction-bonded SiC ceramics, Journal of the Ceramic Society of Japan. 118 (2010) 1028-1031.

[29] M. Wilhelm, W. Wruss. Influence of annealing on the mechanical properties of SiC–Si composites with sub-micron SiC microstructures, Journal of the European Ceramic Society. 20 (2000) 1205-1213.

[30] H.W. Kim, H.E. Kim, H. Song, J. Ha. Effect of Oxidation on the Room- Temperature Flexural Strength of Reaction- Bonded Silicon Carbides, Journal of the American Ceramic Society. 82 (1999) 1601-1604.

[31] Y. Wang, S. Tan, D. Jiang. The effect of porous carbon preform and the infiltration process on the properties of reaction-formed SiC, Carbon. 42 (2004) 1833-1839.

[32] W.J. Xue, T. Ma, Z.P. Xie, J. Yi. Research into mechanical properties of reaction-bonded SiC composites at cryogenic temperatures, Materials Letters. 65 (2011) 3348-3350.

[33] Q.W. Huang, L.H. Zhu. High-temperature strength and toughness behaviors for reaction-bonded SiC ceramics below 1400℃, Materials letters. 59 (2005) 1732-1735.

[34] O.P. Chakrabarti, P.K. Das. High temperature load–deflection behaviour of reaction bonded SiC (RBSC), Ceramics international. 27 (2001) 559-563.

[35] http://www.goodfellow.com

[36] R. Siddheswaran, R. V. Mangalaraja, R. E. Avila, D.Manikandana, C. E. Jeyanthic, S. Ananthakumar. Evaluation of mechanical hardness and fracture toughness of Co and Al co-doped ZnO, Materials Science and Engineering: A. 558 (2012) 456-461.

[37] O. Franke, J.C. Trenkle, C.A. Schuh. Temperature dependence of the indentation size effect, Journal of Materials Research. 25 (2010) 1225-1229.

[38] Y.V. Milman , S. I. Chugunova, I.I. Timofeeva . The resistance of silicon carbide to static and impact local loading[J]. International journal of impact engineering, 2001, 26(1-10): 533-542.

[39] W.C. Oliver, G. M. Pharr. An improved technique for determining hardness and elastic modulus using load and displacement sensing indentation experiments, Journal of materials research. 7 (1992) 1564-1583.

[40] C. H. Kim, A. H. Heuer. A high-temperature displacement-sensitive indenter for studying mechanical properties of thermal barrier coatings, Journal of materials research. 19 (2004) 351-356.

[41] J. Gubicza, A. Juhász, J. Lendvai. A new method for hardness determination from depth sensing indentation tests, Journal of materials research. 11 (1996) 2964-2967.

[42] W. Liu, L.F. Cheng, Y.G. Wang, H.J. Ma. Investigation of the residual stress in reaction-bonded SiC under irradiation, Journal of the European Ceramic Society. 36 (2016) 3901-3907.

[43] R.L.K Matsumoto. Evaluation of Fracture Toughness Determination Methods as Applied to Ceria-Stabilized Tetragonal Zirconia Polycrystal, Journal of the American Ceramic Society. 70 (1987) C366-C368.

[44] A.W. Zia, Z. Zhou, P. W. Shum, L.K.Y. Li. The effect of two-step heat treatment on hardness, fracture toughness, and wear of different biased diamond-like carbon coatings, Surface and Coatings Technology. 320 (2017) 118-125.

[45] K. Niihara. New design concept of structural ceramics, Journal of the Ceramic Society of Japan. 99 (1991) 974-982.

[46] M.C. Chu, S.J. Cho, H.M Park, Y.J. Yoon, H. Ryu. Crack-healing in reaction-bonded silicon carbide, Materials Letters. 58 (2004) 1313-1316.